FERMILAB-PUB-08-295-E

Measurement of $\sigma(p\bar{p} \to Z + X) \cdot \mathrm{Br}(Z \to \tau^+\tau^-)$ at $\sqrt{s} = 1.96$ TeV

V.M. Abazov[36], B. Abbott[75], M. Abolins[65], B.S. Acharya[29], M. Adams[51], T. Adams[49], E. Aguilo[6], M. Ahsan[59], G.D. Alexeev[36], G. Alkhazov[40], A. Alton[64,a], G. Alverson[63], G.A. Alves[2], M. Anastasoaie[35], L.S. Ancu[35], T. Andeen[53], B. Andrieu[17], M.S. Anzelc[53], M. Aoki[50], Y. Arnoud[14], M. Arov[60], M. Arthaud[18], A. Askew[49], B. Åsman[41], A.C.S. Assis Jesus[3], O. Atramentov[49], C. Avila[8], F. Badaud[13], L. Bagby[50], B. Baldin[50], D.V. Bandurin[59], P. Banerjee[29], S. Banerjee[29], E. Barberis[63], A.-F. Barfuss[15], P. Bargassa[80], P. Baringer[58], J. Barreto[2], J.F. Bartlett[50], U. Bassler[18], D. Bauer[43], S. Beale[6], A. Bean[58], M. Begalli[3], M. Begel[73], C. Belanger-Champagne[41], L. Bellantoni[50], A. Bellavance[50], J.A. Benitez[65], S.B. Beri[27], G. Bernardi[17], R. Bernhard[23], I. Bertram[42], M. Besançon[18], R. Beuselinck[43], V.A. Bezzubov[39], P.C. Bhat[50], V. Bhatnagar[27], C. Biscarat[20], G. Blazey[52], F. Blekman[43], S. Blessing[49], K. Bloom[67], A. Boehnlein[50], D. Boline[62], T.A. Bolton[59], E.E. Boos[38], G. Borissov[42], T. Bose[77], A. Brandt[78], R. Brock[65], G. Brooijmans[70], A. Bross[50], D. Brown[81], X.B. Bu[7], N.J. Buchanan[49], D. Buchholz[53], M. Buehler[81], V. Buescher[22], V. Bunichev[38], S. Burdin[42,b], T.H. Burnett[82], C.P. Buszello[43], J.M. Butler[62], P. Calfayan[25], S. Calvet[16], J. Cammin[71], E. Carrera[49], W. Carvalho[3], B.C.K. Casey[50], H. Castilla-Valdez[33], S. Chakrabarti[18], D. Chakraborty[52], K.M. Chan[55], A. Chandra[48], E. Cheu[45], F. Chevallier[14], D.K. Cho[62], S. Choi[32], B. Choudhary[28], L. Christofek[77], T. Christoudias[43], S. Cihangir[50], D. Claes[67], J. Clutter[58], M. Cooke[50], W.E. Cooper[50], M. Corcoran[80], F. Couderc[18], M.-C. Cousinou[15], S. Crépé-Renaudin[14], V. Cuplov[59], D. Cutts[77], M. Ćwiok[30], H. da Motta[2], A. Das[45], G. Davies[43], K. De[78], S.J. de Jong[35], E. De La Cruz-Burelo[33], C. De Oliveira Martins[3], K. DeVaughan[67], J.D. Degenhardt[64], F. Déliot[18], M. Demarteau[50], R. Demina[71], D. Denisov[50], S.P. Denisov[39], S. Desai[50], H.T. Diehl[50], M. Diesburg[50], A. Dominguez[67], H. Dong[72], T. Dorland[82], A. Dubey[28], L.V. Dudko[38], L. Duflot[16], S.R. Dugad[29], D. Duggan[49], A. Duperrin[15], J. Dyer[65], A. Dyshkant[52], M. Eads[67], D. Edmunds[65], J. Ellison[48], V.D. Elvira[50], Y. Enari[77], S. Eno[61], P. Ermolov[38,‡], H. Evans[54], A. Evdokimov[73], V.N. Evdokimov[39], A.V. Ferapontov[59], T. Ferbel[71], F. Fiedler[24], F. Filthaut[35], W. Fisher[50], H.E. Fisk[50], M. Fortner[52], H. Fox[42], S. Fu[50], S. Fuess[50], T. Gadfort[70], C.F. Galea[35], C. Garcia[71], A. Garcia-Bellido[71], V. Gavrilov[37], P. Gay[13], W. Geist[19], W. Geng[15,65], C.E. Gerber[51], Y. Gershtein[49], D. Gillberg[6], G. Ginther[71], N. Gollub[41], B. Gómez[8], A. Goussiou[82], P.D. Grannis[72], H. Greenlee[50], Z.D. Greenwood[60], E.M. Gregores[4], G. Grenier[20], Ph. Gris[13], J.-F. Grivaz[16], A. Grohsjean[25], S. Grünendahl[50], M.W. Grünewald[30], F. Guo[72], J. Guo[72], G. Gutierrez[50], P. Gutierrez[75], A. Haas[70], N.J. Hadley[61], P. Haefner[25], S. Hagopian[49], J. Haley[68], I. Hall[65], R.E. Hall[47], L. Han[7], K. Harder[44], A. Harel[71], J.M. Hauptman[57], J. Hays[43], T. Hebbeker[21], D. Hedin[52], J.G. Hegeman[34], A.P. Heinson[48], U. Heintz[62], C. Hensel[22,d], K. Herner[72], G. Hesketh[63], M.D. Hildreth[55], R. Hirosky[81], J.D. Hobbs[72], B. Hoeneisen[12], H. Hoeth[26], M. Hohlfeld[22], S. Hossain[75], P. Houben[34], Y. Hu[72], Z. Hubacek[10], V. Hynek[9], I. Iashvili[69], R. Illingworth[50], A.S. Ito[50], S. Jabeen[62], M. Jaffré[16], S. Jain[75], K. Jakobs[23], C. Jarvis[61], R. Jesik[43], K. Johns[45], C. Johnson[70], M. Johnson[50], D. Johnston[67], A. Jonckheere[50], P. Jonsson[43], A. Juste[50], E. Kajfasz[15], J.M. Kalk[60], D. Karmanov[38], P.A. Kasper[50], I. Katsanos[70], D. Kau[49], V. Kaushik[78], R. Kehoe[79], S. Kermiche[15], N. Khalatyan[50], A. Khanov[76], A. Kharchilava[69], Y.M. Kharzheev[36], D. Khatidze[70], T.J. Kim[31], M.H. Kirby[53], M. Kirsch[21], B. Klima[50], J.M. Kohli[27], J.-P. Konrath[23], A.V. Kozelov[39], J. Kraus[65], T. Kuhl[24], A. Kumar[69], A. Kupco[11], T. Kurča[20], V.A. Kuzmin[38], J. Kvita[9], F. Lacroix[13], D. Lam[55], S. Lammers[70], G. Landsberg[77], P. Lebrun[20], W.M. Lee[50], A. Leflat[38], J. Lellouch[17], J. Li[78,‡], L. Li[48], Q.Z. Li[50], S.M. Lietti[5], J.K. Lim[31], J.G.R. Lima[52], D. Lincoln[50], J. Linnemann[65], V.V. Lipaev[39], R. Lipton[50], Y. Liu[7], Z. Liu[6], A. Lobodenko[40], M. Lokajicek[11], P. Love[42], H.J. Lubatti[82], R. Luna[3], A.L. Lyon[50], A.K.A. Maciel[2], D. Mackin[80], R.J. Madaras[46], P. Mättig[26], C. Magass[21], A. Magerkurth[64], P.K. Mal[82], H.B. Malbouisson[3], S. Malik[67], V.L. Malyshev[36], Y. Maravin[59], B. Martin[14], R. McCarthy[72], A. Melnitchouk[66], L. Mendoza[8], P.G. Mercadante[5], M. Merkin[38], K.W. Merritt[50], A. Meyer[21], J. Meyer[22,d], J. Mitrevski[70], R.K. Mommsen[44], N.K. Mondal[29], R.W. Moore[6], T. Moulik[58], G.S. Muanza[20], M. Mulhearn[70], O. Mundal[22], L. Mundim[3], E. Nagy[15], M. Naimuddin[50], M. Narain[77], N.A. Naumann[35], H.A. Neal[64], J.P. Negret[8], P. Neustroev[40], H. Nilsen[23], H. Nogima[3], S.F. Novaes[5], T. Nunnemann[25], V. O'Dell[50], D.C. O'Neil[6], G. Obrant[40], C. Ochando[16], D. Onoprienko[59], N. Oshima[50], N. Osman[43], J. Osta[55], R. Otec[10], G.J. Otero y Garzón[50], M. Owen[44], P. Padley[80], M. Pangilinan[77], N. Parashar[56], S.-J. Park[22,d], S.K. Park[31], J. Parsons[70], R. Partridge[77], N. Parua[54], A. Patwa[73], G. Pawloski[80], B. Penning[23], M. Perfilov[38], K. Peters[44], Y. Peters[26], P. Pétroff[16], M. Petteni[43], R. Piegaia[1], J. Piper[65], M.-A. Pleier[22], P.L.M. Podesta-Lerma[33,c], V.M. Podstavkov[50], Y. Pogorelov[55], M.-E. Pol[2], P. Polozov[37],

B.G. Pope[65], A.V. Popov[39], C. Potter[6], W.L. Prado da Silva[3], H.B. Prosper[49], S. Protopopescu[73], J. Qian[64], A. Quadt[22,d], B. Quinn[66], A. Rakitine[42], M.S. Rangel[2], K. Ranjan[28], P.N. Ratoff[42], P. Renkel[79], P. Rich[44], J. Rieger[54], M. Rijssenbeek[72], I. Ripp-Baudot[19], F. Rizatdinova[76], S. Robinson[43], R.F. Rodrigues[3], M. Rominsky[75], C. Royon[18], P. Rubinov[50], R. Ruchti[55], G. Safronov[37], G. Sajot[14], A. Sánchez-Hernández[33], M.P. Sanders[17], B. Sanghi[50], G. Savage[50], L. Sawyer[60], T. Scanlon[43], D. Schaile[25], R.D. Schamberger[72], Y. Scheglov[40], H. Schellman[53], T. Schliephake[26], S. Schlobohm[82], C. Schwanenberger[44], A. Schwartzman[68], R. Schwienhorst[65], J. Sekaric[49], H. Severini[75], E. Shabalina[51], M. Shamim[59], V. Shary[18], A.A. Shchukin[39], R.K. Shivpuri[28], V. Siccardi[19], V. Simak[10], V. Sirotenko[50], P. Skubic[75], P. Slattery[71], D. Smirnov[55], G.R. Snow[67], J. Snow[74], S. Snyder[73], S. Söldner-Rembold[44], L. Sonnenschein[17], A. Sopczak[42], M. Sosebee[78], K. Soustruznik[9], B. Spurlock[78], J. Stark[14], J. Steele[60], V. Stolin[37], D.A. Stoyanova[39], J. Strandberg[64], S. Strandberg[41], M.A. Strang[69], E. Strauss[72], M. Strauss[75], R. Ströhmer[25], D. Strom[53], L. Stutte[50], S. Sumowidagdo[49], P. Svoisky[55], A. Sznajder[3], P. Tamburello[45], A. Tanasijczuk[1], W. Taylor[6], B. Tiller[25], F. Tissandier[13], M. Titov[18], V.V. Tokmenin[36], I. Torchiani[23], D. Tsybychev[72], B. Tuchming[18], C. Tully[68], P.M. Tuts[70], R. Unalan[65], L. Uvarov[40], S. Uvarov[40], S. Uzunyan[52], B. Vachon[6], P.J. van den Berg[34], R. Van Kooten[54], W.M. van Leeuwen[34], N. Varelas[51], E.W. Varnes[45], I.A. Vasilyev[39], P. Verdier[20], L.S. Vertogradov[36], M. Verzocchi[50], D. Vilanova[18], F. Villeneuve-Seguier[43], P. Vint[43], P. Vokac[10], M. Voutilainen[67,e], R. Wagner[68], H.D. Wahl[49], M.H.L.S. Wang[50], J. Warchol[55], G. Watts[82], M. Wayne[55], G. Weber[24], M. Weber[50,f], L. Welty-Rieger[54], A. Wenger[23,g], N. Wermes[22], M. Wetstein[61], A. White[78], D. Wicke[26], M. Williams[42], G.W. Wilson[58], S.J. Wimpenny[48], M. Wobisch[60], D.R. Wood[63], T.R. Wyatt[44], Y. Xie[77], S. Yacoob[53], R. Yamada[50], W.-C. Yang[44], T. Yasuda[50], Y.A. Yatsunenko[36], H. Yin[7], K. Yip[73], H.D. Yoo[77], S.W. Youn[53], J. Yu[78], C. Zeitnitz[26], S. Zelitch[81], T. Zhao[82], B. Zhou[64], J. Zhu[72], M. Zielinski[71], D. Zieminska[54], A. Zieminski[54,‡], L. Zivkovic[70], V. Zutshi[52], and E.G. Zverev[38]

(The DØ Collaboration)

[1] *Universidad de Buenos Aires, Buenos Aires, Argentina*
[2] *LAFEX, Centro Brasileiro de Pesquisas Físicas, Rio de Janeiro, Brazil*
[3] *Universidade do Estado do Rio de Janeiro, Rio de Janeiro, Brazil*
[4] *Universidade Federal do ABC, Santo André, Brazil*
[5] *Instituto de Física Teórica, Universidade Estadual Paulista, São Paulo, Brazil*
[6] *University of Alberta, Edmonton, Alberta, Canada, Simon Fraser University, Burnaby, British Columbia, Canada, York University, Toronto, Ontario, Canada, and McGill University, Montreal, Quebec, Canada*
[7] *University of Science and Technology of China, Hefei, People's Republic of China*
[8] *Universidad de los Andes, Bogotá, Colombia*
[9] *Center for Particle Physics, Charles University, Prague, Czech Republic*
[10] *Czech Technical University, Prague, Czech Republic*
[11] *Center for Particle Physics, Institute of Physics, Academy of Sciences of the Czech Republic, Prague, Czech Republic*
[12] *Universidad San Francisco de Quito, Quito, Ecuador*
[13] *LPC, Université Blaise Pascal, CNRS/IN2P3, Clermont, France*
[14] *LPSC, Université Joseph Fourier Grenoble 1, CNRS/IN2P3, Institut National Polytechnique de Grenoble, Grenoble, France*
[15] *CPPM, Aix-Marseille Université, CNRS/IN2P3, Marseille, France*
[16] *LAL, Université Paris-Sud, IN2P3/CNRS, Orsay, France*
[17] *LPNHE, IN2P3/CNRS, Universités Paris VI and VII, Paris, France*
[18] *CEA, Irfu, SPP, Saclay, France*
[19] *IPHC, Université Louis Pasteur, CNRS/IN2P3, Strasbourg, France*
[20] *IPNL, Université Lyon 1, CNRS/IN2P3, Villeurbanne, France and Université de Lyon, Lyon, France*
[21] *III. Physikalisches Institut A, RWTH Aachen University, Aachen, Germany*
[22] *Physikalisches Institut, Universität Bonn, Bonn, Germany*
[23] *Physikalisches Institut, Universität Freiburg, Freiburg, Germany*
[24] *Institut für Physik, Universität Mainz, Mainz, Germany*
[25] *Ludwig-Maximilians-Universität München, München, Germany*
[26] *Fachbereich Physik, University of Wuppertal, Wuppertal, Germany*
[27] *Panjab University, Chandigarh, India*
[28] *Delhi University, Delhi, India*
[29] *Tata Institute of Fundamental Research, Mumbai, India*
[30] *University College Dublin, Dublin, Ireland*

[31]*Korea Detector Laboratory, Korea University, Seoul, Korea*
[32]*SungKyunKwan University, Suwon, Korea*
[33]*CINVESTAV, Mexico City, Mexico*
[34]*FOM-Institute NIKHEF and University of Amsterdam/NIKHEF, Amsterdam, The Netherlands*
[35]*Radboud University Nijmegen/NIKHEF, Nijmegen, The Netherlands*
[36]*Joint Institute for Nuclear Research, Dubna, Russia*
[37]*Institute for Theoretical and Experimental Physics, Moscow, Russia*
[38]*Moscow State University, Moscow, Russia*
[39]*Institute for High Energy Physics, Protvino, Russia*
[40]*Petersburg Nuclear Physics Institute, St. Petersburg, Russia*
[41]*Lund University, Lund, Sweden, Royal Institute of Technology and Stockholm University, Stockholm, Sweden, and Uppsala University, Uppsala, Sweden*
[42]*Lancaster University, Lancaster, United Kingdom*
[43]*Imperial College, London, United Kingdom*
[44]*University of Manchester, Manchester, United Kingdom*
[45]*University of Arizona, Tucson, Arizona 85721, USA*
[46]*Lawrence Berkeley National Laboratory and University of California, Berkeley, California 94720, USA*
[47]*California State University, Fresno, California 93740, USA*
[48]*University of California, Riverside, California 92521, USA*
[49]*Florida State University, Tallahassee, Florida 32306, USA*
[50]*Fermi National Accelerator Laboratory, Batavia, Illinois 60510, USA*
[51]*University of Illinois at Chicago, Chicago, Illinois 60607, USA*
[52]*Northern Illinois University, DeKalb, Illinois 60115, USA*
[53]*Northwestern University, Evanston, Illinois 60208, USA*
[54]*Indiana University, Bloomington, Indiana 47405, USA*
[55]*University of Notre Dame, Notre Dame, Indiana 46556, USA*
[56]*Purdue University Calumet, Hammond, Indiana 46323, USA*
[57]*Iowa State University, Ames, Iowa 50011, USA*
[58]*University of Kansas, Lawrence, Kansas 66045, USA*
[59]*Kansas State University, Manhattan, Kansas 66506, USA*
[60]*Louisiana Tech University, Ruston, Louisiana 71272, USA*
[61]*University of Maryland, College Park, Maryland 20742, USA*
[62]*Boston University, Boston, Massachusetts 02215, USA*
[63]*Northeastern University, Boston, Massachusetts 02115, USA*
[64]*University of Michigan, Ann Arbor, Michigan 48109, USA*
[65]*Michigan State University, East Lansing, Michigan 48824, USA*
[66]*University of Mississippi, University, Mississippi 38677, USA*
[67]*University of Nebraska, Lincoln, Nebraska 68588, USA*
[68]*Princeton University, Princeton, New Jersey 08544, USA*
[69]*State University of New York, Buffalo, New York 14260, USA*
[70]*Columbia University, New York, New York 10027, USA*
[71]*University of Rochester, Rochester, New York 14627, USA*
[72]*State University of New York, Stony Brook, New York 11794, USA*
[73]*Brookhaven National Laboratory, Upton, New York 11973, USA*
[74]*Langston University, Langston, Oklahoma 73050, USA*
[75]*University of Oklahoma, Norman, Oklahoma 73019, USA*
[76]*Oklahoma State University, Stillwater, Oklahoma 74078, USA*
[77]*Brown University, Providence, Rhode Island 02912, USA*
[78]*University of Texas, Arlington, Texas 76019, USA*
[79]*Southern Methodist University, Dallas, Texas 75275, USA*
[80]*Rice University, Houston, Texas 77005, USA*
[81]*University of Virginia, Charlottesville, Virginia 22901, USA and*
[82]*University of Washington, Seattle, Washington 98195, USA*

(Dated: August 8, 2008)

We present a measurement of the cross section for Z boson production times the branching fraction to tau lepton pairs $\sigma(p\bar{p} \to Z + X) \cdot \mathrm{Br}(Z \to \tau^+\tau^-)$ in $p\bar{p}$ collisions at $\sqrt{s} = 1.96$ TeV. The measurement is performed in the channel in which one tau lepton decays into a muon and neutrinos, and the other tau lepton decays hadronically or into an electron and neutrinos. The data sample corresponds to an integrated luminosity of 1.0 fb^{-1} collected with the D0 detector at the Fermilab Tevatron Collider. The sample contains 1511 candidate events with an estimated 20% background from jets or muons misidentified as tau leptons. We obtain $\sigma \cdot \mathrm{Br} = 240 \pm 8\,(\mathrm{stat}) \pm 12\,(\mathrm{sys}) \pm 15\,(\mathrm{lum})$ pb, which is consistent with the standard model prediction.

PACS numbers: 13.38.Dg, 13.85.Qk

The resonant production of tau lepton pairs is as interesting for the study of standard model (SM) physics as the production of lighter lepton pairs. For new phenomena, especially for decays of particles coupled to mass, such as SM or supersymmetric Higgs bosons, the detection of resonant pairs of tau leptons becomes even more interesting. This is due to the fact that tau leptons are much heavier than the other leptons, increasing the chance that these new phenomena would be observed first in this channel. Unfortunately, the detection of tau leptons is far more difficult than that of muons or electrons.

A measurement of $\sigma(p\bar{p} \to Z + X)\cdot\mathrm{Br}(Z \to \tau^+\tau^-)$ in $p\bar{p}$ collisions at $\sqrt{s} = 1.96$ TeV is described in this Letter. The analysis is based on an event sample containing a single isolated muon from a tau lepton decay and a tau candidate reconstructed as a narrow jet that could be produced by a tau lepton decaying either hadronically or into an electron and neutrinos. This measurement is of interest not only as a test of the SM prediction but also because any excess over the expected $\sigma\cdot$Br could be an indication of a source other than Z bosons for events containing tau lepton pairs, such as the Higgs boson [1]. The precision of this result is significantly improved compared to earlier publications [2, 3].

The analysis presented here is based on data collected between September 2002 and February 2006 by the D0 experiment, corresponding to an integrated luminosity of 1003 ± 62 pb^{-1} [4].

The D0 detector [5] is a general purpose, axially and forward-backward symetric detector, consisting of a central-tracking system located within a 2 T superconducting solenoidal magnet, surrounded by three liquid-argon/uranium calorimeters and a muon detector. The spatial coordinates of the D0 detector are defined using a righthanded Cartesian system with the origin in the center of the detector. The positive z-axis is the direction of the proton beam, the positive y-axis points upwards and the positive x-axis points out of the Tevatron ring. The azimuthal angle ϕ is measured with respect to the positive x direction. Pseudorapidity is defined as $\eta = -\ln[\tan(\theta/2)]$, where the polar angle θ is measured with respect to the positive z direction. The tracking system has coverage up to $\eta \approx 3$. The calorimeter consists of a central section (CC) covering $|\eta| \lesssim 1.1$ and two end calorimeters (EC) that extend coverage to $|\eta| \approx 4.2$, all housed in separate cryostats and segmented into cells of dimensions 0.1×0.1 in $\eta - \phi$ space [6]. The muon system [7] provides a coverage up to $\eta \approx 2$ and is located outside the calorimeter; it consists of a layer of tracking detectors and scintillation trigger counters before 1.8 T iron toroids, followed by two similar layers after the toroids. Luminosity is measured using plastic scintillator arrays located in front of the EC cryostats, covering $2.7 < |\eta| < 4.4$. A three level trigger system is designed to select most interesting events based on preliminary information from the tracking, calorimetry, and muon systems, reducing the number of recorded events from the collision rate of ≈ 2 MHz to a rate of ≈ 50 Hz, which is written to tape.

The triggering strategy used in this analysis is based on the tau lepton which decays into $\mu\nu_\mu\nu_\tau$. A single muon trigger requiring hits in the muon system in combination with a high transverse momentum (p_T) track reconstructed in the central tracking system is required. The average trigger efficiency, ultimately parametrized as a function of ϕ, η and z using a data sample of $Z \to \mu^+\mu^-$ events, is $(52.3 \pm 1.4)\%$. No dependence on the muon p_T is observed above 15 GeV.

Most backgrounds as well as the efficiency of the selection for signal $Z \to \tau^+\tau^-$ events are estimated using Monte Carlo (MC) simulations. All simulated samples are generated with PYTHIA [8] using the CTEQ6.1L parton distribution function (PDF) set. Simulation of the D0 detector is done using GEANT3 [9]. Noise in the detector and the contributions from other simultaneous interactions are simulated by adding random untriggered data events to the MC simulation. These events were chosen such that the effective instantaneous luminosity distribution in MC is the same as in data. The code used for the reconstruction of simulated events is identical to the one used for data.

Corrections are applied to all MC events to obtain overall good agreement between the simulation and collider data. The momentum scale and resolution for muons in the MC are tuned to reproduce the Z boson invariant mass distribution observed in data. Similarly, the jet energy resolution is tuned to match that observed in data for each region of the detector. The p_T spectrum of the Z boson for events generated with PYTHIA has a different shape than that measured in data; therefore the p_T of the Z boson is reweighted to fit the direct measurement in data [10]. Small differences in acceptance between data and simulation are corrected for by weighting the simulated z position of the primary vertex in MC events to reproduce that observed in data.

Reconstruction efficiencies for muons and tracks are calculated both in data and MC using samples of $Z \to \mu^+\mu^-$ events. Efficiency correction factors for MC events as a function of muon or track ϕ, η and z are applied. The signal or background samples are normalized to the expected number of events evaluated using the luminosity of the data sample and the theoretical values of the next-to-next-to-leading order (NNLO) cross sections in the case of Z boson production [11, 12] or next-to-leading order (NLO) cross sections for all other processes where

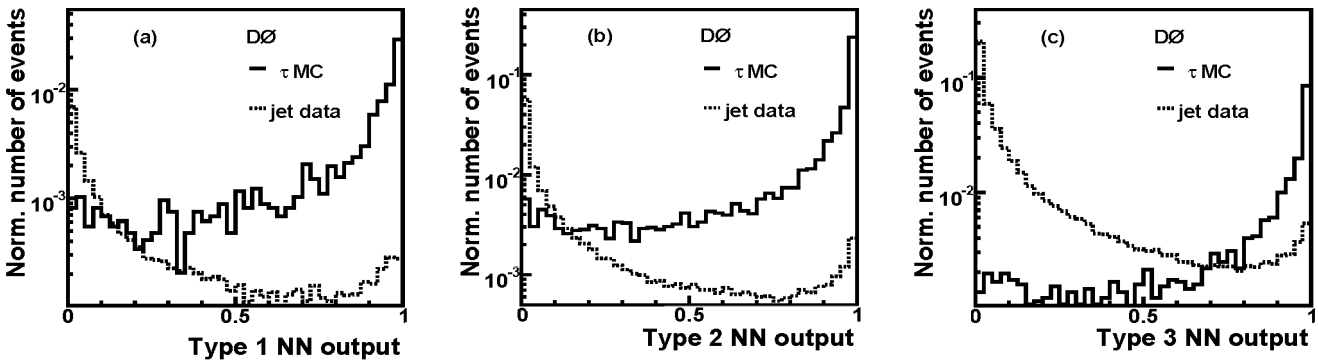

FIG. 1: NN output distributions for (a) type 1, (b) type 2, and (c) type 3 tau candidates. The ratio of signal to background is arbitrary, but the relative amounts of type 1, type 2, and type 3 events in background and signal are not. The distributions are normalized with respect to each other such that the sum over the three types is 1 for both signal and background.

the NNLO calculation is not available. W boson production is normalized from data.

In this analysis, muons are identified starting with their signature in the muon detector. The track reconstructed from hits in the muon layers is required to match a track from the central tracking detectors. The muon momentum is measured using only the central tracking detectors.

A tau candidate is a collection of (i) a calorimeter cluster reconstructed using a simple cone algorithm [13], (ii) tracks associated with the calorimeter cluster of which at least one has $p_T > 1.5$ GeV but with a total invariant mass less than 1.8 GeV, and (iii) electromagnetic (EM) sub-clusters constructed from the cells in the EM section of the calorimeter. The size of the cone used for reconstruction of the calorimeter cluster is $\mathcal{R} = \sqrt{(\Delta\phi)^2 + (\Delta\eta)^2} = 0.5$, where $\Delta\phi$ is the difference in azimuthal angle, and $\Delta\eta$ the difference in pseudorapidity between the cone axis and each of the calorimeter towers. Isolation variables are calculated using a cone of $\mathcal{R} = 0.3$. The tracks associated with the tau candidate must also be contained within this $\mathcal{R} = 0.3$ cone.

Tau candidates are classified as type 1, 2 or 3, depending on the numbers of tracks and EM sub-clusters they possess. Type 1 tau candidates have exactly one associated track and no EM sub-clusters, type 2 have one associated track and one or more EM sub-clusters, and type 3 have at least two associated tracks. These categories correspond roughly to pure one-prong decays, one-prong plus neutral pion decays as well as decay into electrons, and three-prong decays of the tau lepton.

Due to the large number of jets reconstructed as tau candidates, additional selection criteria must be applied in order to distinguish tau leptons from jets. Three neural networks (NN), one for each tau type, are trained using $Z \to \tau^+\tau^-$ MC events as signal and events with a jet back-to-back with a non-isolated muon from data as background. The NNs use isolation variables based on tracks, hadronic and EM calorimeter clusters, as well as shower shape variables and correlation variables between calorimeter and tracks. Figure 1 shows the discrimination obtained using the NNs. Requiring that the NN output be larger than 0.9 results in a background rejection of almost a factor of 50 for all three tau types. This reduces the probability for a jet to be misidentified as a tau lepton to 1.1% for the sum of all types (from 52% without the NN output requirement), while maintaining a total efficiency of close to 70% for tau leptons which decay hadronically or to an electron and neutrinos. Electrons are treated as type 2 tau candidates, since the efficiency for them to be reconstructed as such and pass the NN output requirement is 98%. For a complete description of the neural networks and details on their performance see Ref. [14].

The variable chosen to best illustrate the $Z \to \tau^+\tau^-$ signal is the visible mass, given by:

$$\text{Visible Mass} = \sqrt{(\mathrm{P}_\mu + \mathrm{P}_\tau + \not\mathrm{P}_\mathrm{T})^2}, \qquad (1)$$

where $\mathrm{P}_{\mu,\tau} = (E_{\mu,\tau}, p^x_{\mu,\tau}, p^y_{\mu,\tau}, p^z_{\mu,\tau})$ are the four-momentum vectors of the muon and the tau candidate, and $\not\mathrm{P}_T = (\not\!\!E_T, \not\!\!E^x_T, \not\!\!E^y_T, 0)$, with $\not\!\!E_T$ being the missing transverse energy in the event and $\not\!\!E^x_T, \not\!\!E^y_T$ being its projections along the x and y directions. The uncorrected missing transverse energy is defined as the vector equal in length and opposite in direction to the vectorial sum of transverse energies of the calorimeter cells. The transverse momenta of muons are subtracted from this vector, after corrections for the energy deposited by the muons in the calorimeter have been applied. When the tau candidate matches a reconstructed electron, the energy corrections derived for electrons are applied. For jets corresponding to tau candidates, the tau energy corrections described below are applied. Jet energy corrections applied to all other jets in the event are propagated to the missing E_T calculation.

To compare the visible mass distributions of the tau pairs between data and MC, it is important to have the correct energy scale for the tau candidate. For type 1 tau candidates, the momentum of the track is used as the best estimate of the energy of the tau candidate when the tracking resolution is superior to the calorimeter energy resolution (up to calorimeter cluster energy of 70 GeV). For type 2 candidates matching electrons, the energy corrections derived for electrons are applied. For type 2 candidates not matching electrons and type 3 tau candidates, the energy is estimated using

$$E^{\rm corr} = \sum_i p_i^{\rm trk} + E^{\rm cal} - \sum_i R(p_i^{\rm trk}, \eta) \cdot p_i^{\rm trk}, \qquad (2)$$

where $p_i^{\rm trk}$ is the momentum of track i associated with the tau candidate, $E^{\rm cal}$ is the energy deposited by the tau candidate in the calorimeter, and $R(p_i^{\rm trk}, \eta)$ represents the response of the calorimeter to the $\pi^{\pm}$ which produced track i associated with the tau candidate, as a function of the energy and rapidity of the $\pi^{\pm}$. Typically, $0.6 < R(p_i^{trk}, \eta) < 0.9$. As the resolution of the calorimeter is better than that of the tracking at calorimeter cluster energies higher than 70 GeV (type 1), 100 GeV (type 2), or 120 GeV (type 3), the energy of the calorimeter cluster is used in these cases, after applying η and energy dependent corrections obtained from MC.

The default program in the D0 GEANT simulation for hadronic interactions, GEISHA [15], does not reproduce the charged pion response in data well. Therefore GCALOR [16] is used for a more precise simulation of single charged pion interactions. The charged pion response obtained using these special simulations was found to be in reasonable agreement with preliminary data measurements in the central calorimeter [17]. The energy measurement for neutral particles, mostly important for type 2 taus, is dominated by electromagnetic showers in the calorimeter. The simulation of electromagnetic showers in GEANT is sufficiently accurate for the purpose of this measurement.

The preselection requires one isolated muon reconstructed within the pseudorapidity interval $|\eta| < 1.6$. The transverse momentum of the muon as measured by the central tracking detectors must satisfy $p_T^{\mu} > 15$ GeV. No other muon matched to a central track with $p_T > 10$ GeV is allowed in the event. The muon isolation requires the sum of energies of all cells situated in a hollow cone around the direction of the muon with $0.1 < \mathcal{R} < 0.4$, as well as the sum of all tracks in a cone of $\mathcal{R} < 0.5$, excluding the muon track, to be less than 2.5 GeV.

The preselection further requires one tau candidate with $p_T > 15$ GeV, $|\eta| < 2$, scalar sum of the transverse momenta of all tracks associated with the tau candidate > 15 GeV for types 1 and 3 and > 5 GeV for type 2 tau candidates, $NN > 0.3$, and no other muon matching the tau candidate. Type 3 tau candidates with two tracks are only considered if both tracks have the same charge. The tau candidate is required to have a charge with opposite sign to that of the muon. The distances in the z direction at the track's point of closest approach between the muon and the primary vertex, the tau candidate and the primary vertex, as well as the distance between the muon and the tau candidate must be less than 1 cm.

In total 8316 events pass these criteria. To reduce the W + jets and the $Z \to \mu^+\mu^-$ backgrounds, another selection criterion is used, based on a variable which gives an approximation of the W boson mass, referred to as m^*:

$$m^* = \sqrt{2E_\nu E_\mu (1 - \cos\Delta\phi)}, \qquad (3)$$

where $E_\nu = \not\!\!E_T \cdot E_\mu / p_T^\mu$ is an approximation of the neutrino energy, and $\Delta\phi$ is the angle between $\not\!\!E_T$ and the muon in the transverse plane.

For the final selection, all the preselection criteria are applied. Additionally, the lower limit on the NN output for the tau candidates is raised to 0.9 for types 1 and 2, and to 0.95 for type 3 tau candidates. The final selection also requires $m^* < 20$ GeV. A total of 1511 events pass all the selection criteria.

The dominant remaining background arises from multijet processes, mainly from $b\bar{b}$ events where the muon isolation requirement is met and one of the jets satisfies the tau candidate selection criteria. Another significant source of events with isolated muons and tau candidates is W + jets production, where the W boson decays to $\mu\nu$ and one of the jets is misidentified as a tau candidate. The $Z \to \mu^+\mu^-$ background is reduced by the requirement that no other muon be found in the event, but a small number of events will be selected when one of the muons is not reconstructed. Small contributions are also expected from $W \to \tau\nu$ and $WW \to l\nu l\nu$, as well as $t\bar{t}$ production. Contributions from WZ and ZZ events yield less than one event each after the final selection criteria and are therefore neglected. All backgrounds, except the multijet background, are estimated using MC simulations.

The multijet background is estimated using the data events that satisfy all requirements placed on the signal sample except that the muon and the tau candidate have the same sign charge. We call this the same-sign (SS) sample. To obtain the appropriate normalization for this background, a special data sample is selected, the "multijet sample," containing events that pass all requirements placed on the signal sample except the isolation criteria and the cut on the tau NN output. Instead of the isolation requirement used for the signal events, the events in the multijet sample have the sum of energies of all calorimeter cells inside the hollow isolation cone in the range 2.5 to 10 GeV. The sum of all non-muon tracks p_T within the track isolation cone is required to be in the same interval $2.5 - 10$ GeV. To avoid contamination from

$Z \to \tau^+\tau^-$ signal events, an upper limit on the tau NN output is placed at 0.8. To increase the statistics of this sample, the muon p_T is required to be at least 10 GeV instead of 15 GeV. The multijet sample is expected to be completely dominated by multijet processes, but may also include events in which a W decaying into a muon is produced in association with a jet. The W + jets contribution is reduced by requiring that the muon and the tau candidate are back to back ($|\phi_\mu - \phi_\tau| > 2.5$). A slight excess of opposite sign (OS) over SS events is observed in the multijet sample. No significant dependence of the OS/SS ratio as a function of p_T or NN output is observed for the three types of tau candidates in the multijet sample. Correction factors ($f^i_{\rm mj}$) of $1.13 \pm 0.03, 1.08 \pm 0.01$, and 1.06 ± 0.01 for tau types 1 to 3 are obtained, being used as discussed below to normalize the multijet background in the final signal sample.

The number of events in the SS sample is corrected for the contribution from $Z \to \mu^+\mu^-$, $Z \to \tau^+\tau^-$, and $W \to \tau\nu$ obtained from MC, multiplied by an additional correction factor which takes into account the difference between the charge misidentification rates in data and MC. Totals of 6 events for type 1, 16 events for type 2, and 18 events for type 3 tau candidates from $Z \to \mu^+\mu^-$, $Z \to \tau^+\tau^-$, and $W \to \tau\nu$ are estimated to have a misidentified charge after all cuts and are subtracted from the number of SS events when the multijet background is calculated. The contribution from $W \to \mu\nu$ events is accounted for separately.

A part of the W + jets background is already included in the SS sample. However, we expect a significant excess of OS events compared to the number of SS events due to the fact that a high percentage of $W+1$ jet events comes from quark jets. The number of W+jets events in data is estimated by selecting a sample that is expected to have a large contribution from W boson processes and low or negligible contributions from Z boson production. Such a W+jets enriched sample can be obtained by requiring an isolated muon with $p_T > 20$ GeV, a tau candidate with $0.3 < NN < 0.8$, $|\phi_\mu - \phi_\tau| < 2.7$, and $m^* > 40$ GeV. Mostly multijet and W+jets events contribute to this sample. The excess of OS events compared to SS events is given for the multijet background by $f^i_{\rm mj}$ for tau type i. For the W + jets sample, similar factors (f^i_W) of $2.39 \pm 1.01, 3.15 \pm 1.17$, and 1.6 ± 0.26 are estimated from data, in the sample with the cuts listed above, but requiring a tighter cut $m^* > 60$ GeV. Using this, we can calculate the number of W + jets events in the W + jets enriched data sample by solving the following system of two equations for each tau type i:

$$N^i_W + N^i_{\rm mj} = N^i_{OS} + N^i_{SS} \tag{4}$$

$$\frac{f^i_W - 1}{f^i_W + 1} N^i_W + \frac{f^i_{\rm mj} - 1}{f^i_{\rm mj} + 1} N^i_{\rm mj} = N^i_{OS} - N^i_{SS} \tag{5}$$

where N^i_W is the number of W + jets events, $N^i_{\rm mj}$ is the number of multijet events and N^i_{OS}, N^i_{SS} are the numbers of OS, respectively SS events in the W + jets enriched data sample. The ratios between the number of W + jets events calculated in data by solving the above system of equations and the one expected from MC for each tau type are used as normalization factors for this background in the signal region. The uncertainty on N^i_W from data is taken as a systematic uncertainty. The estimated number of W + jets events in the signal sample, not including those in the SS sample, is 14 ± 5 events.

Several distributions such as muon and tau candidate transverse momentum, pseudorapidity, and azimuthal angle, as well as $\not\!\!E_T$, m^*, and visible mass are compared between the data and the predicted sum of backgrounds and $Z \to \tau^+\tau^-$ for the SM cross section and branching ratio. All these distributions show good agreement after each of the preselection, NN selection, and anti-W requirement stages.

In Fig. 2 the visible mass distribution for events which pass the final selection requirements is shown separately for each of the tau types, while Fig. 3 shows the same distribution for the sum of all types. Good agreement is observed between the data and the sum of the background SM processes and $Z \to \tau^+\tau^-$ signal, normalized using the NNLO SM prediction [11, 12].

Table I shows the number of events expected for each tau type from each of the backgrounds, as well as from the $Z \to \tau^+\tau^-$ signal. It also shows the total numbers of expected background and signal events in comparison to the numbers of events observed in data for three levels of selection: preselection, preselection plus NN output requirement, and after all selection criteria are applied. Good agreement is observed between the predicted and observed numbers of events at each level of selection for all tau types.

We estimate that approximately 1.2% of all $Z \to \tau^+\tau^-$ events have the wrong sign for either the muon or the tau candidate, therefore appearing as SS events. From the number of $Z \to \tau^+\tau^-$ events obtained by subtracting the estimated background from the number of events in the final sample, we calculate the number of $Z \to \tau^+\tau^-$ events reconstructed as SS to be 17. This number is added to the number of events in the OS sample when calculating the $Z \to \tau^+\tau^-$ cross section.

Reconstruction of a second track close to a first reconstructed track is found to be more efficient in MC than in data. A correction factor of 0.97 ± 0.028 is applied to simulated events containing type 3 tau candidates. This factor is obtained by comparing the ratios of type 3 tau candidates with two and three tracks in data and MC and taking into account that there are twice as many SS as OS combinations when one of the three tracks is lost.

Systematic uncertainties on the multijet and W + jets backgrounds are derived from the statistical uncertainties of the control samples used to estimate these backgrounds

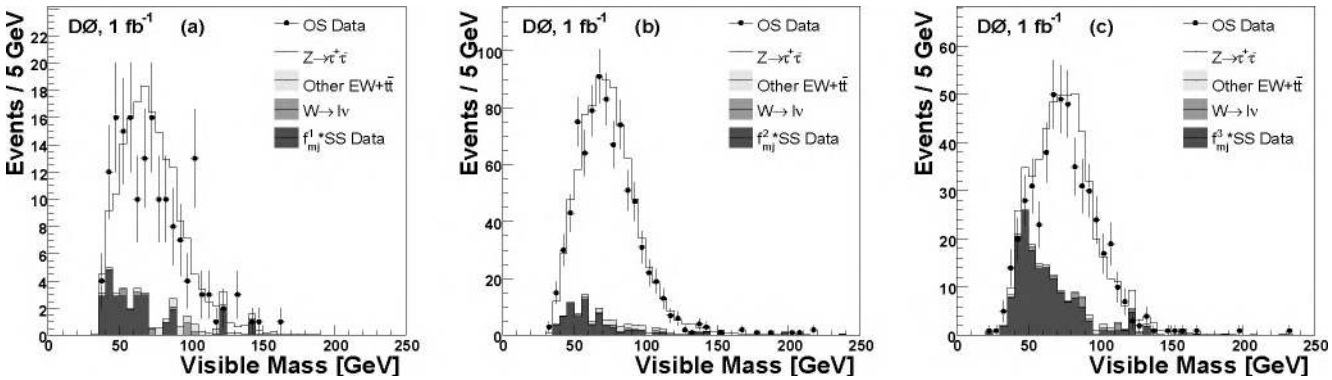

FIG. 2: Visible mass distribution for (a) type 1 tau events, (b) type 2 tau events, and (c) type 3 tau events. The data are the points with error bars. The different components of the SM expectation are as given in the legend. The $Z \to \tau^+\tau^-$ signal is normalized to the theoretical expectation calculated at NNLO using MRST2004 PDFs [11, 12].

	Type 1			Type 2			Type 3		
Process	Preselection	Preselection + NN > 0.9	All cuts	Preselection	Preselection + NN > 0.9	All cuts	Preselection	Preselection + NN > 0.95	All cuts
$Z/\gamma^* \to \tau^+\tau^-$	302 ± 4	230 ± 4	146 ± 3	1469 ± 9	1131 ± 8	786 ± 7	693 ± 6	484 ± 5	358 ± 5
$Z/\gamma^* \to \mu^+\mu^-$	58 ± 2	43 ± 2	6.1 ± 0.6	176 ± 3	108 ± 3	14.0 ± 0.8	184 ± 3	38 ± 1	8.9 ± 0.7
WW	7.2 ± 0.3	6.1 ± 0.3	0.4 ± 0.1	79 ± 1	74 ± 1	6.9 ± 0.3	9.3 ± 0.4	6.1 ± 0.5	0.5 ± 0.1
$t\bar{t}$	2.7 ± 0.3	2.0 ± 0.3	0.2 ± 0.1	33 ± 1	28 ± 1	2.4 ± 0.3	29 ± 1	4.2 ± 0.4	0.5 ± 0.1
$W \to \tau\nu$	10 ± 2	4 ± 1	1.5 ± 0.8	50 ± 4	14.1 ± 2.2	1.4 ± 0.7	168 ± 7	22.0 ± 2.7	3.7 ± 1.2
$W \to \mu\nu$	127 ± 11	42 ± 5	2.1 ± 0.9	470 ± 18	116 ± 9	6.7 ± 1.9	1384 ± 32	202 ± 13	14.1 ± 2.7
Multijet	208 ± 15	46 ± 8	25 ± 5	584 ± 25	123 ± 12	61 ± 8	2265 ± 47	273 ± 18	145 ± 13
Predicted	715 ± 18	373 ± 11	181 ± 7	2861 ± 32	1594 ± 18	878 ± 12	4732 ± 59	1029 ± 23	531 ± 15
Data	720	380	170	2836	1546	843	4760	981	498

TABLE I: Number of OS events expected for each tau type from the $Z \to \tau^+\tau^-$ signal as well as from each of the backgrounds, their sum and the number of OS events observed in data, for three levels of selection: preselection, preselection + NN output > 0.9 (0.95 for type 3) and after all selection criteria are applied (preselection + NN output > 0.9 or $0.95 + m^* < 20$ GeV). The uncertainies are statistical.

and from the systematic uncertainties on the correction factors used for their normalization.

The systematic uncertainty related to the tau energy measurement is estimated by scaling the charged pion response used for data by the largest difference found between the response measured in data and the response obtained using GCALOR (6%) and recalculating the acceptance applying all cuts. The value of this uncertainty is 1%.

NN systematic uncertainties are calculated using statistical ensembles of events in which each input variable is allowed to fluctuate within the difference observed between the distributions of that particular variable in data and MC. The RMS of the ratio of the number of events passing a certain NN cut to the number of events in the ensembles, called the ensemble cut ratio, is taken as a measure of the NN uncertainty. The estimated uncertainties are 4.3% for type 1, 2.0% for type 2, and 3.8% for type 3 tau candidates, which results in a total uncertainty of 2.7%.

The uncertainty due to the tau candidate track reconstruction efficiency is taken to be the same as the uncertainty on reconstructing muon tracks and is estimated using $Z \to \mu^+\mu^-$ events to be 1.4%. The uncertainty on the correction factor due to differences between data and MC in tracking efficiency for type 3 taus is added in quadrature to this value, resulting in a total uncertainty related to the tau candidate tracks of 1.6%. The systematic uncertainties due to muon identification and muon track matching are determined to be 0.6% and 0.8%, respectively. The systematic uncertainty due to the charge misidentification is 1%. The uncertainty on the trigger efficiency is 2.7% and takes into account the bias related to the choice of the control sample, the variation due to possible background contamination, variations in time or due to changing luminosity, the choice of binning, and the choice of parameters for the efficiency, as well as the limited statistics. The uncertainty on the total integrated luminosity is 6.1% [4], with an additional systematic uncertainty of 1% related to the influence on the luminosity of applying the data quality criteria used to reject events with coherent calorimeter noise.

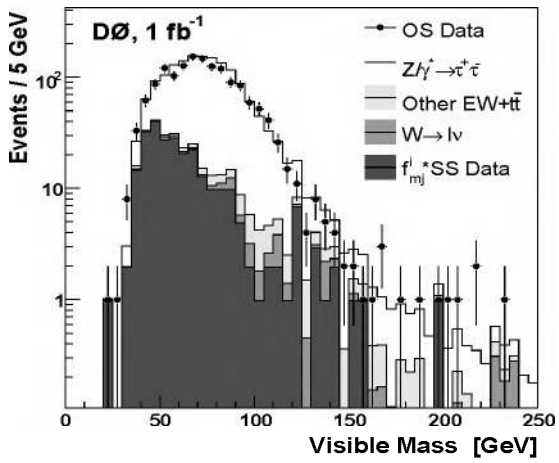

FIG. 3: Visible mass distribution for all tau types. The $Z \to \tau^+\tau^-$ signal is normalized to the theoretical expectation calculated at NNLO using MRST2004 PDFs.

The PDF uncertainty of 2.0% is estimated using a NLO calculation [19] and the CTEQ6.1 error sets. This uncertainty is obtained from the variation in acceptance when these error sets are used, added in quadrature with the difference in acceptance when using the MRST2004 error sets at NLO and with the additional variation when going from NLO to NNLO with MRST2004. Table II summarizes all the systematic uncertainties.

Source	Value
Tau energy scale	1.0 %
Tau identification	2.7 %
Tau track reconstruction	1.6 %
Multijet background	1.6 %
$W \to \mu\nu$ background	0.5 %
Trigger	2.7 %
Muon track match	0.8 %
Muon identification	0.6 %
Muon momentum resolution	0.4 %
Charge misidentification	1.0 %
MC statistics	0.6 %
PDF	2.0 %
Total (except luminosity)	5.2 %
Luminosity	6.2 %

TABLE II: Systematic uncertainties on the $\sigma(p\bar{p} \to Z/\gamma^* + X) \cdot \mathrm{Br}(Z/\gamma^* \to \tau^+\tau^-)$ measurement.

The cross section times branching ratio for the process $p\bar{p} \to Z/\gamma^* + X \to \tau^+\tau^- + X$ is given by the number of signal events divided by the product of the total efficiency and the integrated luminosity. The number of signal events estimated from Table I, with the correction for signal events reconstructed as SS, is 1227. Since Table I shows the estimated number of events in the Z/γ^* mass range $15 - 500$ GeV, other corrections have to be made in order to compare the result of this analysis with theoretical cross sections. To limit the mass range to $60 - 130$ GeV, the number of events expected from the mass region $15 - 60$ GeV (7 events) as well as from the $130 - 500$ GeV mass region (26 events) are subtracted from the number of signal events in data. The total efficiency for $Z \to \tau^+\tau^-$ events in the $60 - 130$ GeV mass region is 4.9×10^{-3}, which also includes the trigger efficiency of 52.3%. Finally, a factor of 0.98 [20] is applied to estimate the Z boson cross section as opposed to the Z/γ^* cross section for this mass region.

Given the systematic uncertainties listed in Table II and an integrated luminosity of 1003 pb^{-1}, we estimate $\sigma(p\bar{p} \to Z + X) \cdot \mathrm{Br}(Z \to \tau^+\tau^-) = 240 \pm 8$ (stat) $\pm$ 12 (sys) $\pm$ 15 (lum) pb, which is in good agreement with the SM prediction of $251.9^{+5.0}_{-11.8}$ pb [11, 12] that results from the NNLO calculation using the MRST2004 PDFs, as well as with the $241.6^{+3.6}_{-3.2}$ pb [11, 18] value obtained at NNLO using the CTEQ6.1M PDF parametrization. This result is the most precise measurement of $\sigma(p\bar{p} \to Z + X) \cdot \mathrm{Br}(Z \to \tau^+\tau^-)$ to date, in good agreement with previous measurements of the Z boson cross section times branching ratio to leptons at $\sqrt{s} = 1.96$ TeV [2, 3, 21].

We thank the staffs at Fermilab and collaborating institutions, and acknowledge support from the DOE and NSF (USA); CEA and CNRS/IN2P3 (France); FASI, Rosatom and RFBR (Russia); CNPq, FAPERJ, FAPESP and FUNDUNESP (Brazil); DAE and DST (India); Colciencias (Colombia); CONACyT (Mexico); KRF and KOSEF (Korea); CONICET and UBACyT (Argentina); FOM (The Netherlands); STFC (United Kingdom); MSMT and GACR (Czech Republic); CRC Program, CFI, NSERC and WestGrid Project (Canada); BMBF and DFG (Germany); SFI (Ireland); The Swedish Research Council (Sweden); CAS and CNSF (China); and the Alexander von Humboldt Foundation (Germany).

[a] Visitor from Augustana College, Sioux Falls, SD, USA.
[b] Visitor from The University of Liverpool, Liverpool, UK.
[c] Visitor from ECFM, Universidad Autonoma de Sinaloa, Culiacán, Mexico.
[d] Visitor from II. Physikalisches Institut, Georg-August-University, Göttingen, Germany.
[e] Visitor from Helsinki Institute of Physics, Helsinki, Finland.
[f] Visitor from Universität Bern, Bern, Switzerland.
[g] Visitor from Universität Zürich, Zürich, Switzerland.
[‡] Deceased.

[1] D0 Collaboration, V.M. Abazov *et al.*, Phys. Rev. Lett. **97**, 121802 (2006); D0 Collaboration, V.M. Abazov *et al.*, arXiv:0805.2941 (2008), accepted by Phys. Rev. Lett.
[2] D0 Collaboration, V.M. Abazov *et al.*, Phys. Rev. D **71**, 072004 (2005); Erratum Phys. Rev. D **77**, 039901(E) (2008).
[3] CDF Collaboration, A. Abulencia *et al.*, Phys. Rev. D

75, 092004 (2007).
[4] T. Andeen *et. al.*, FERMILAB-TM-2365 (2007).
[5] D0 Collaboration, V.M. Abazov *et al.*, Nucl. Instrum. Methods Phys. Res. A **565**, 463 (2006).
[6] D0 Collaboration, S. Abachi *et al.*, Nucl. Instrum. Methods Phys. Res. A **338**, 185 (1994).
[7] D0 Collaboration, V.M. Abazov *et al.*, Nucl. Instrum. Methods Phys. Res. A **552**, 372 (2005).
[8] T. Sjöstrand *et al.*, Comput. Phys. Commun. **135**, 238 (2001). The version used was 6.323.
[9] R. Brun and F. Carminati, CERN Program Library Long Writeup W5013, 1993 (unpublished).
[10] D0 Collaboration, V.M. Abazov *et al.*, Phys. Rev. Lett. **100**, 102002 (2008).
[11] R. Hamberg, W.L. van Neerven, and T. Matsuura, Nucl. Phys. **B359**, 343 (1991); Erratum ibid **B644**, 403 (2002). An additional description of uncertainties can be found in arXiv:hep-ph/0308087 (2003).
[12] A.D. Martin, R.G. Roberts, W.J. Stirling, and R.S. Thorne, Phys. Lett. B **604**, 61 (2004).
[13] G. Blazey *et al.*, arXiv:hep-ex/0005012v2 (2000).
[14] C.F. Galea, Proc. "Physics at LHC 2006, Cracow, Poland," Acta Physica Polon. **B38**, 769 (2007).
[15] H.C. Fesefeldt, University of Aachen Technical Report PITHA 85-02 (1985).
[16] C. Zeitnitz and A. Gabriel, "The GEANT-Calor Interface User's Guide" ORNL, Oak Ridge (1996).
[17] C.F. Galea, PhD thesis, FERMILAB-THESIS-2008-22.
[18] J. Pumplin *et al.*, JHEP **0207**, 012 (2002); D. Stump *et al.*, JHEP **0310**, 046 (2003).
[19] K. Melnikov and F. Petriello, Phys. Rev.D **74**, 114017 (2006); C. Anastasiou, L.J. Dixon, K. Melnikov, and F. Petriello, Phys. Rev. D **69**, 094008 (2004).
[20] S. Frixione and B.R. Webber, JHEP **06**, 029 (2002).
[21] CDF Collaboration, D. Acosta *et al.*, Phys. Rev. Lett. **94**, 091803 (2005).